Astro/Physics 224 Winter 2008

Origin and Evolution of the Universe

Dark Halos

Lecture 10 - Friday Feb 15

Joel Primack

University of California, Santa Cruz

Outline

1. large-scale structure: CDM

2. dark halos: collapse & mergers

3. luminous galaxies in dark halos

4. puzzles in galaxy formation

H. J. Mo, S.D.M. White
MNRAS 336 (2002) 112

The abundance and clustering of dark haloes in the standard Lambda CDM cosmogony

We define the characteristic properties of a dark halo within a sphere of radius r200 chosen so that the mean enclosed density is 200 times the mean cosmic value. Then

$$r_{200} = \left[\frac{GM}{100\Omega_{\rm m}(z)H^2(z)}\right]^{1/3}, \quad \text{and} \quad V_c = \left(\frac{GM}{r_{200}}\right)^{1/2}, \; R(M) \equiv \left(\frac{3M}{4\pi\overline{\rho}_0}\right)^{1/3}, \; \sigma^2(R) = \frac{1}{2\pi^2}\int_0^\infty k^3 P(k)\tilde{W}^2(kR)\frac{{\rm d}k}{k},$$

According to the argument first given by Press & Schechter (1974, hereafter PS), the abundance of haloes as a function of mass and redshift, expressed as the number of haloes per unit comoving volume at redshift z with mass in the interval $(M, M+dM)$, may be written as

$$n(M,z){\rm d}M = \sqrt{\frac{2}{\pi}}\frac{\overline{\rho}_0}{M}\frac{{\rm d}\nu}{{\rm d}M}\exp\left(-\frac{\nu^2}{2}\right){\rm d}M\,. \tag{9}$$

Here $\nu \equiv \delta_c/[D(z)\sigma(M)]$, where $\delta_c \approx 1.69$ and the growth factor is $D(z) = g(z)/[g(0)(1+z)]$ with

$$g(z) \approx \frac{5}{2}\Omega_{\rm m}\left[\Omega_{\rm m}^{4/7} - \Omega_\Lambda + (1+\Omega_{\rm m}/2)(1+\Omega_\Lambda/70)\right]^{-1}, \; \Omega_{\rm m} \equiv \Omega_{\rm m}(z), \quad \Omega_\Lambda \equiv \Omega_\Lambda(z) = \frac{\Omega_{\Lambda,0}}{E^2(z)}\,.$$

Lahav, Lilje, Primack, & Rees 1991

$$E(z) = \left[\Omega_{\Lambda,0} + (1-\Omega_0)(1+z)^2 + \Omega_{\rm m,0}(1+z)^3\right]^{\frac{1}{2}}\,.$$

Press & Schechter derived the above mass function from the *Ansatz* that the fraction F of all cosmic mass which at redshift z is in haloes with masses exceeding M is *twice* the fraction of randomly placed spheres of radius $R(M)$ which have linear overdensity at that time exceeding δ_c, the value at which a spherical perturbation collapses. Since the linear fluctuation distribution is gaussian this hypothesis implies

$$F(>M,z) = {\rm erfc}\left(\frac{\nu}{\sqrt{2}}\right), \tag{12}$$

and equation (9) then follows by differentiation.

The PS formula is $$n(M,z)\mathrm{d}M = \sqrt{\frac{2}{\pi}}\frac{\overline{\rho}_0}{M}\frac{\mathrm{d}\nu}{\mathrm{d}M}\exp\left(-\frac{\nu^2}{2}\right)\mathrm{d}M \tag{9}$$

Numerical simulations show that although the scaling properties implied by the PS argument hold remarkably well for a wide variety of hierarchical cosmogonies, substantially better fits to simulated mass functions are obtained if the error function in equation (12) is replaced by a function of slightly different shape. Sheth & Tormen (1999) suggested the following modification of equation (9)

$$n(M,z)\mathrm{d}M = A\left(1+\frac{1}{\nu'^{2q}}\right)\sqrt{\frac{2}{\pi}}\frac{\overline{\rho}}{M}\frac{\mathrm{d}\nu'}{\mathrm{d}M}\exp\left(-\frac{\nu'^2}{2}\right)\mathrm{d}M, \tag{14}$$

where $\nu' = \sqrt{a}\nu$, $a = 0.707$, $A \approx 0.322$ and $q = 0.3$.

[See Sheth, Mo & Tormen (2001) and Sheth & Tormen (2002) for a justification of this formula in terms of an ellipsoidal model for perturbation collapse.] The fraction of all matter in haloes with mass exceeding M can be obtained by integrating equation (14). To good approximation,

$$F(>M,z) \approx 0.4\left(1+\frac{0.4}{\nu^{0.4}}\right)\mathrm{erfc}\left(\frac{0.85\nu}{\sqrt{2}}\right)$$

In a detailed comparison with a wide range of simulations, Jenkins et al. (2001) confirmed that this model is indeed a good fit provided haloes are defined at the same density contrast relative to the mean in all cosmologies.

Improved Press-Schechter Halo Number Density

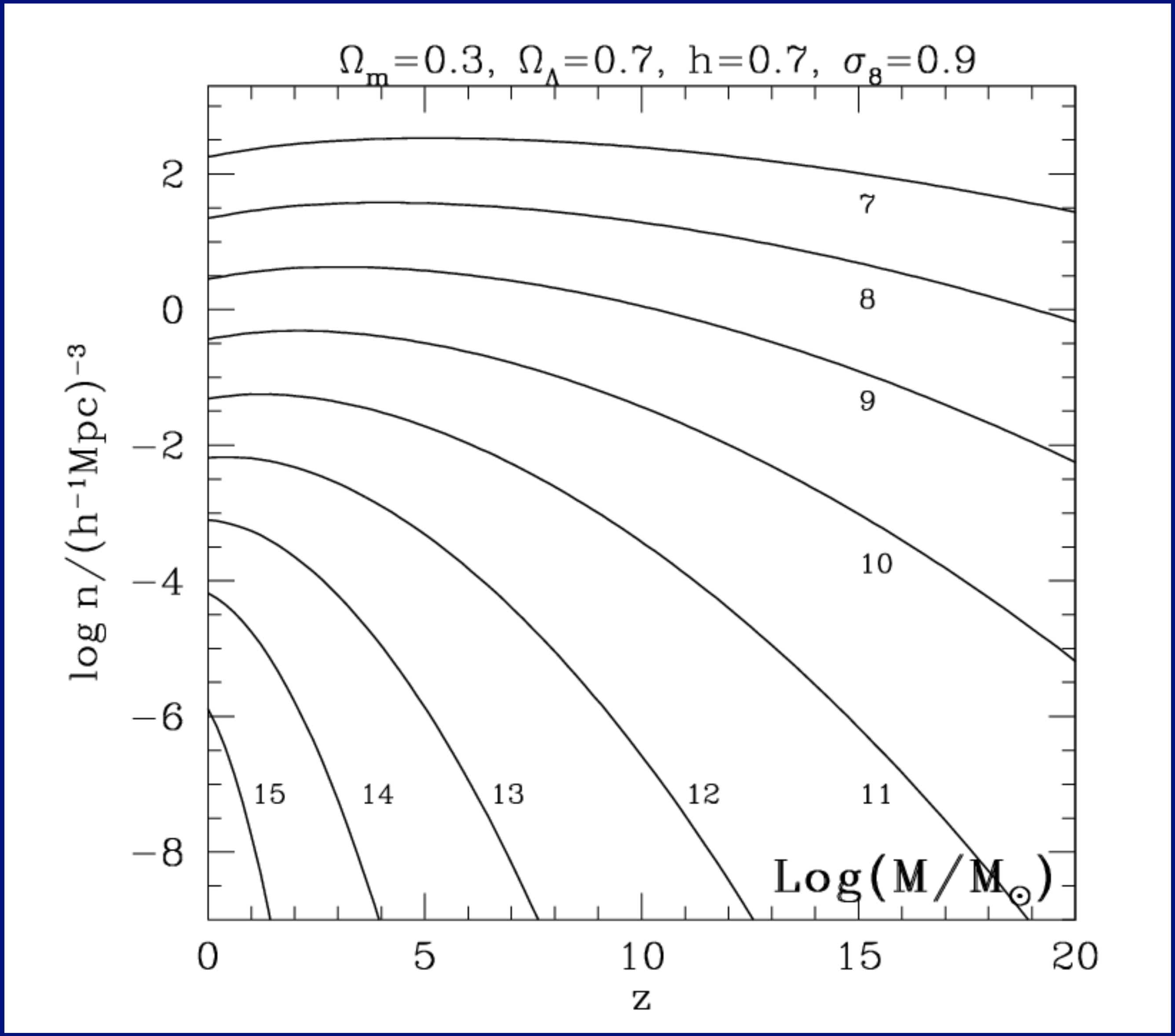

Mo & White 2002

Comoving Halo Number Density vs. Mass

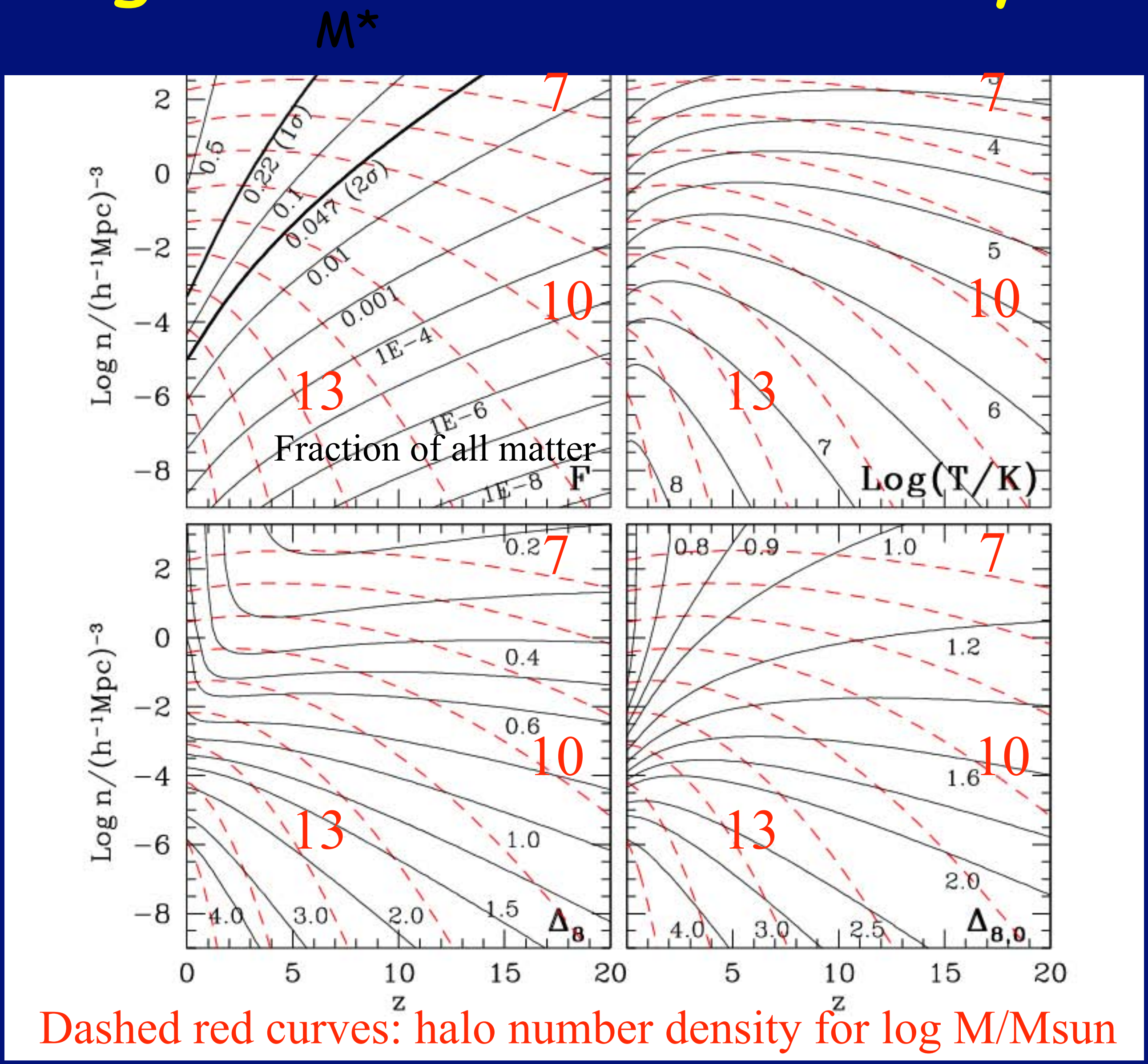

Standard LCDM

Mo & White 2002

Cosmological Simulation Methods

Dissipationless Simulations

Particle-Particle (PP) - Aarseth NbodyN, N=1,...,6
Particle Mesh (PM) - see Klypin & Holtzman 1997
Adaptive PM (P3M) - Efstathiou et al.
Tree - Barnes & Hut 1986, PKDGRAV Stadel
TreePM - GADGET2, Springel 2005
Adaptive Mesh Refinement (AMR) - Klypin (ART)

Hydrodynamical Simulations

Fixed grid - Cen & Ostriker
Smooth Particle Hydrodynamics (SPH) - GADGET2, Springel 2005
- Gasoline, Wadsley, Stadel, & Quinn
Adaptive grid - ART+hydro - Klypin & Kravtsov

Initial Conditions

Standard: Gaussian P(k) realized uniformly, Zel'dovich displacement
Multimass - put lower mass particles in a small part of sim volume
Constrained realization - small scale: simulate individual halos (NFW)
large scale: simulate particular region

Reviews

Bertschinger ARAA 1998, Klypin lectures 2002, U Washington website

Structure of Dark Matter Halos

Navarro, Frenk, White
1996 1997 →

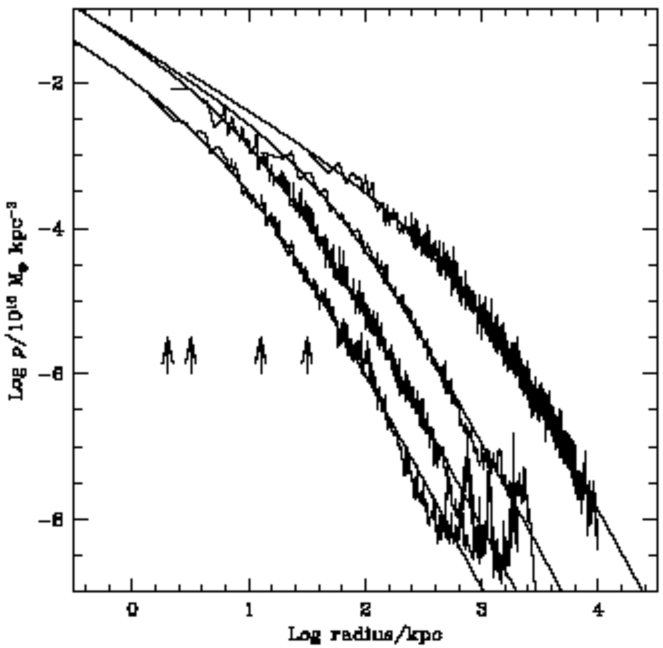

Fig. 3.— Density profiles of four halos spanning four orders of magnitude in mass. The arrows indicate the gravitational softening, h_g, of each simulation. Also shown are fits from eq.3. The fits are good over two decades in radius, approximately from h_g out to the virial radius of each system.

$$\frac{\rho(r)}{\rho_{crit}} = \frac{\delta_c}{(r/r_s)(1+r/r_s)^2}, \qquad (3)$$

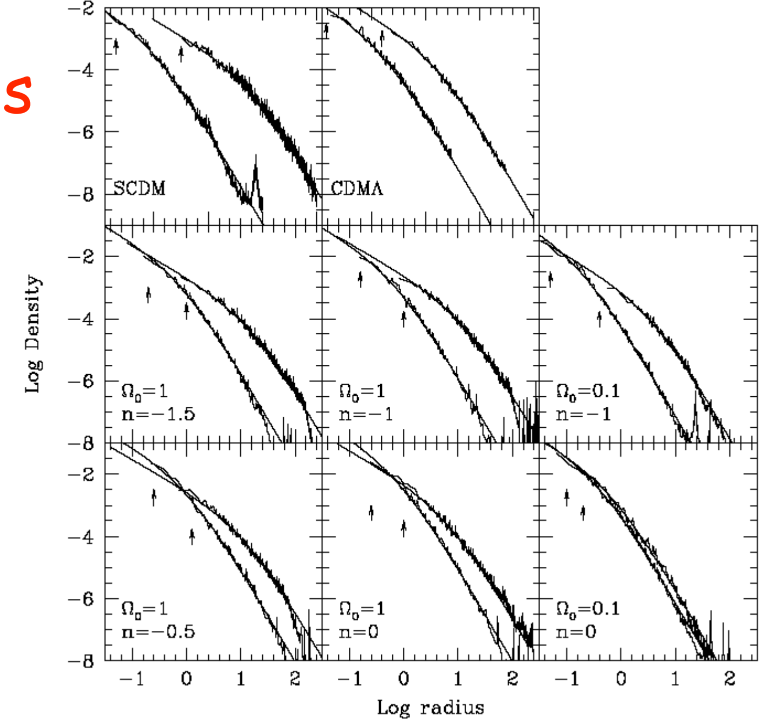

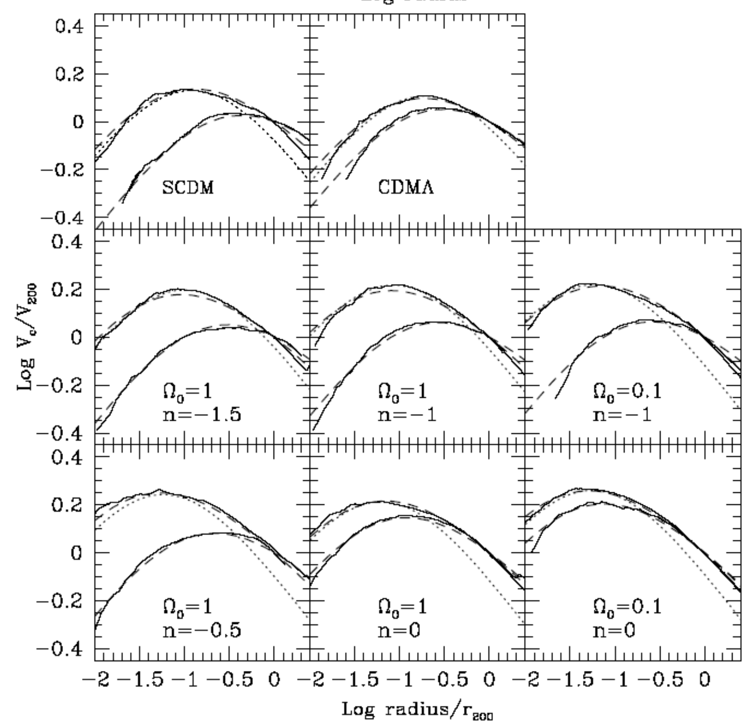

NFW formula works for <u>all</u> models

Dark Matter Halo Radial Profile

Comparison of NFW and Moore et al. profiles

Parameter	NFW	Moore et al.
Density $x = r/r_s$	$\rho = \dfrac{\rho_s}{x(1+x)^2}$ $\rho \propto x^{-3}$ for $x \gg 1$ $\rho \propto x^{-1}$ for $x \ll 1$ $\rho/\rho_s = 1/4$ at $x = 1$	$\rho = \dfrac{\rho_s}{x^{1.5}(1+x)^{1.5}}$ $\rho \propto x^{-3}$ for $x \gg 1$ $\rho \propto x^{-1.5}$ for $x \ll 1$ $\rho/\rho_s = 1/2$ at $x = 1$
Mass $M = 4\pi\rho_s r_s^3 f(x)$ $= M_{\rm vir} f(x)/f(C)$ $M_{\rm vir} = \frac{4\pi}{3}\rho_{\rm cr}\Omega_0\delta_{\rm top-hat} r_{\rm vir}^3$	$f(x) = \ln(1+x) - \dfrac{x}{1+x}$	$f(x) = \frac{2}{3}\ln(1+x^{3/2})$
Concentration $C = r_{\rm vir}/r_s$	$C_{\rm NFW} = 1.72 C_{\rm Moore}$ for halos with the same $M_{\rm vir}$ and $r_{\rm max}$ $C_{1/5} \approx \dfrac{C_{\rm NFW}}{0.86 f(C_{\rm NFW}) + 0.1363}$ error less than 3% for $C_{\rm NFW}$ =5-30 $C_{\gamma=-2} = C_{\rm NFW}$	$C_{\rm Moore} = C_{\rm NFW}/1.72$ $C_{1/5} = \dfrac{C_{\rm Moore}}{[(1+C_{\rm Moore}^{3/2})^{1/5} - 1]^{2/3}}$ $\approx \dfrac{C_{\rm Moore}}{[C_{\rm Moore}^{3/10} - 1]^{2/3}}$ $C_{\gamma=-2} = 2^{3/2} C_{\rm Moore}$ $\approx 2.83 C_{\rm Moore}$
Circular Velocity $v_{\rm circ}^2 = \dfrac{GM_{\rm vir}}{r_{\rm vir}} \dfrac{C}{x} \dfrac{f(x)}{f(C)}$ $= v_{\rm max}^2 \dfrac{x_{\rm max}}{x} \dfrac{f(x)}{f(x_{\rm max})}$ $v_{\rm vir}^2 = \dfrac{GM_{\rm vir}}{r_{\rm vir}}$	$x_{\rm max} \approx 2.15$ $v_{\rm max}^2 \approx 0.216 v_{\rm vir}^2 \dfrac{C}{f(C)}$ $\rho/\rho_s \approx 1/21.3$ at $x = 2.15$	$x_{\rm max} \approx 1.25$ $v_{\rm max}^2 \approx 0.466 v_{\rm vir}^2 \dfrac{C}{f(C)}$ $\rho/\rho_s \approx 1/3.35$ at $x = 1.25$

Klypin, Kravtsov, Bullock & Primack 2001

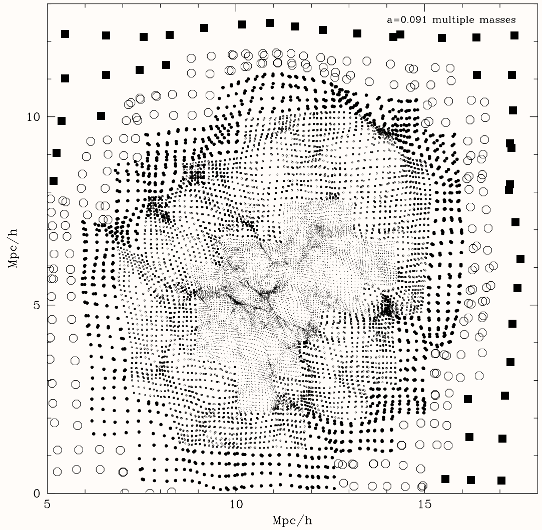

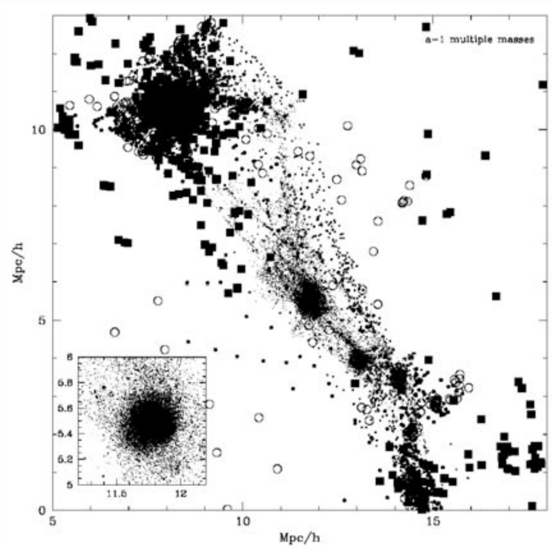

Fig. 2.— Distribution of particles of different masses in a thin slice through the center of halo A_1 (see Table 1) at $z = 10$ (top panel) and at $z = 0$ (bottom panel). To avoid crowding of points the thickness of the slice is made smaller in the center (about $30h^{-1}$kpc) and larger ($1h^{-1}$Mpc) in the outer parts of the forming halo. Particles of different mass are shown with different symbols: tiny dots, dots, large dots, squares, and open circles.

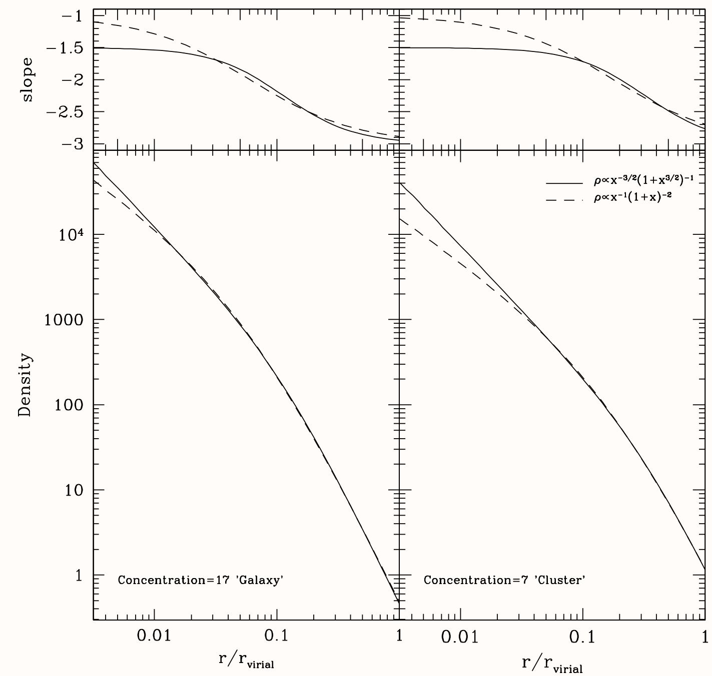

Fig. 3.— Comparison of the Moore et al. and the NFW profiles. Each profile is normalized to have the same virial mass and the same radius of the maximum circular velocity. *Left panels:* High-concentration halo typical of small galaxy-size halos $C_{\rm NFW} = 17$. *Right panels:* Low-concentration halo typical of cluster-size halos. The deviations are very small ($< 3\%$) for radii $r > r_s/2$. Top panels show the local logarithmic slope of the profiles. Note that for the high concentration halo the slope of the profile is significantly larger than the asymptotic value -1 even at very small radii $r \approx 0.01 r_{\rm vir}$.

Klypin, Kravtsov,
Bullock & Primack 2001

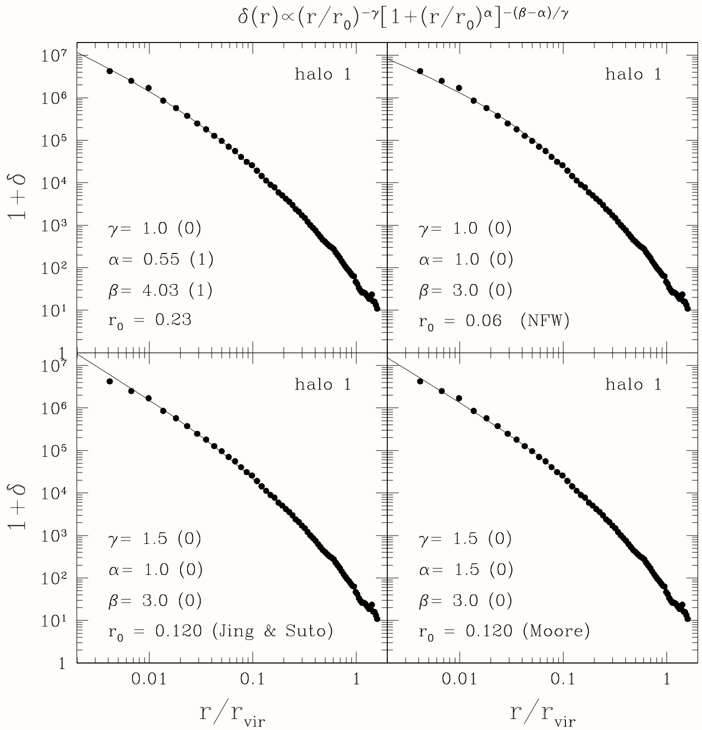

Fig. 8.— Analytic fits to the density profile of the halo A_1 from our set of simulations. The fits are of the form $\rho(r) \propto (r/r_0)^{-\gamma}[1 + (r/r_0)^{\alpha}]^{-(\beta-\alpha)/\gamma}$. The legend in each panel indicates the corresponding values of α, β, and γ of the fit; the digit in parenthesis indicates whether the parameter was kept fixed (0) or not (1) during the fit. Note that various sets of parameters α, β, γ provide equally good fits to the simulated halo profile in the whole range resolved range of scales $\approx 0.005 - 1r_{\rm vir}$. This indicates a large degree of degeneracy in parameters α, β, and γ

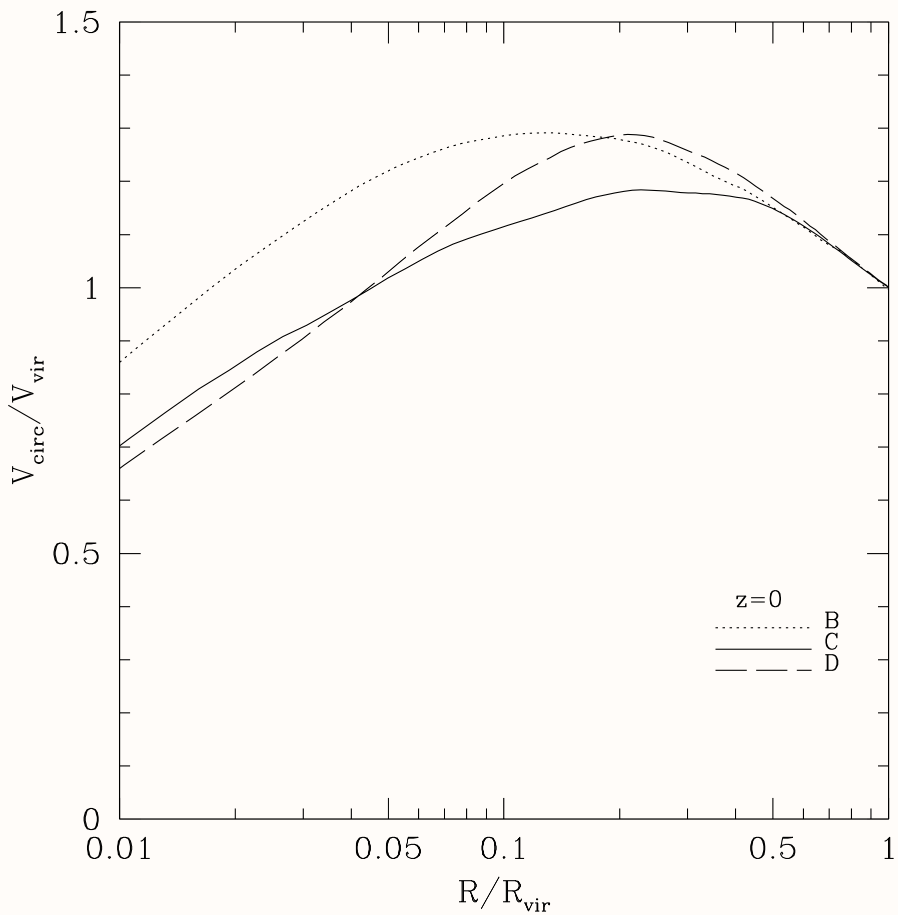

Fig. 9.— Circular velocity profiles for the halos B_1, C_1, and D_1 normalized to halo's virial velocity. Halos are well resolved on all shown scales. Although the halos have very similar masses, the profiles are very different; the differences are due to real differences in the concentration parameters.

Klypin, Kravtsov, Bullock & Primack 2001

Empirical Models for Dark Matter Halos. II. Inner profile slopes, dynamical profiles, and ρ/σ^3

Alister Graham, David Merritt, Ben Moore, Jürg Diemand, Balša Terzić

Einasto's model is given by the equation

$$\rho(r) = \rho_e \exp\left\{-d_n\left[(r/r_e)^{1/n} - 1\right]\right\}.$$

Data on log slopes from innermost resolved radius of observed galaxies, not corrected for observational effects -- adapted from de Blok (2004).

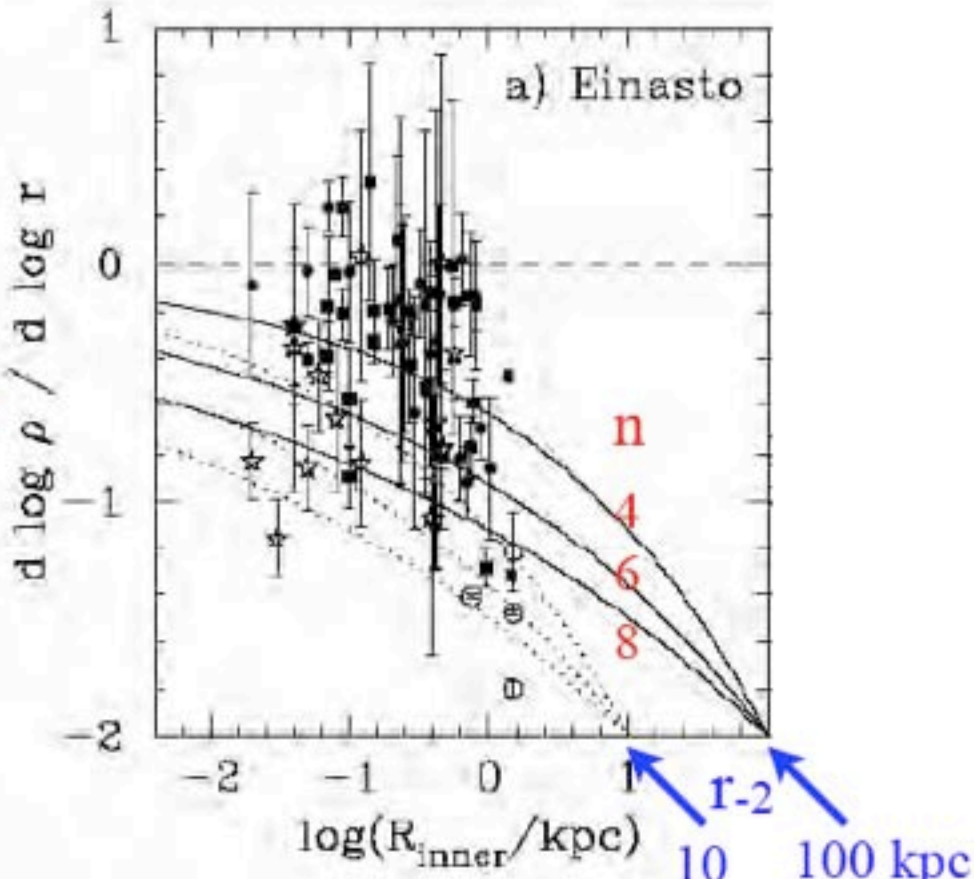

Evolution of Halo Maximum Circular Velocity

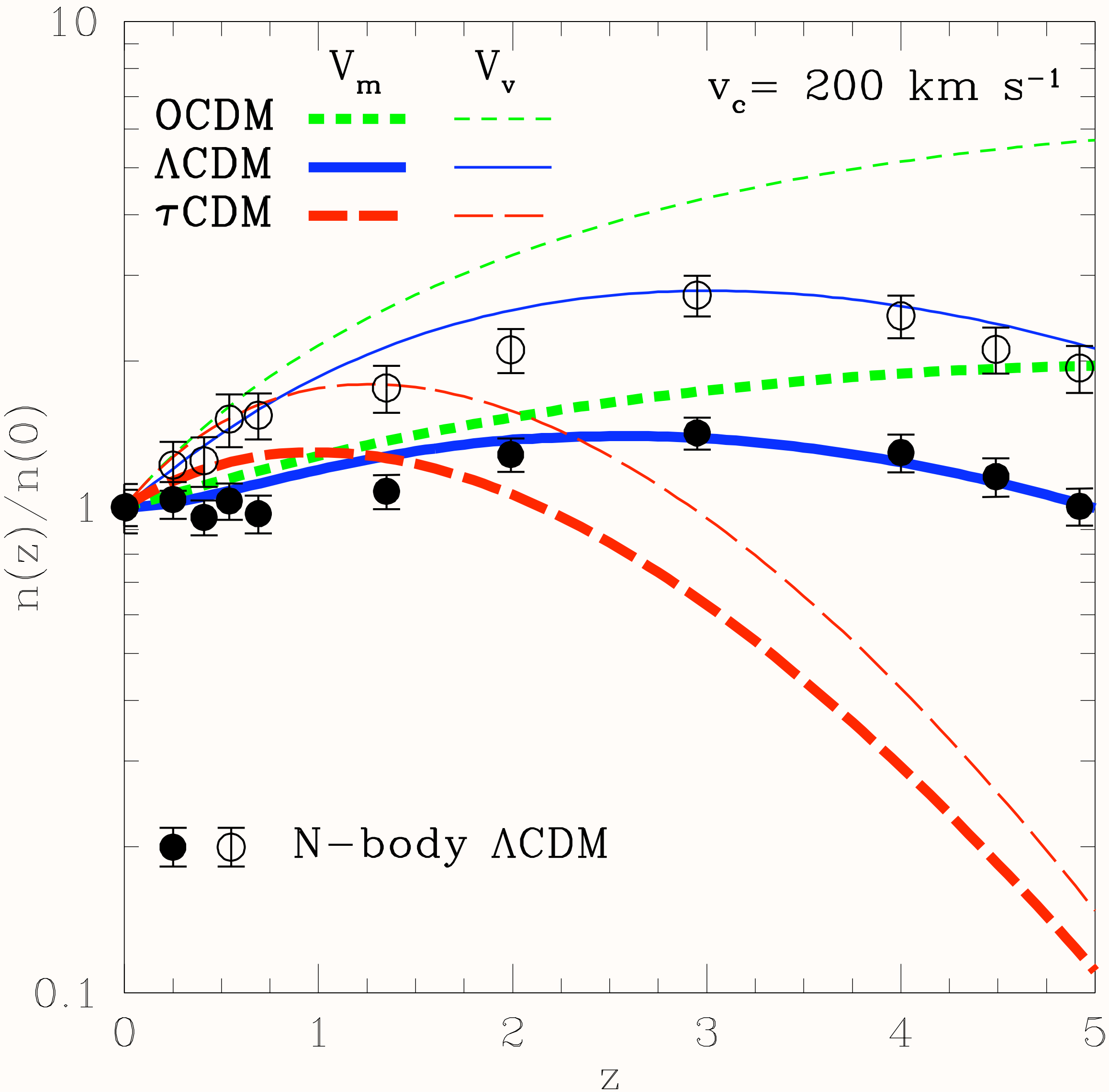

FIG. 1.— Evolution of relative comoving number density for fixed $v_m = 200\,\mathrm{km\,s^{-1}}$ (bold curves) and $v_v = 200\,\mathrm{km\,s^{-1}}$ halos in three cosmologies.

Bullock, Dekel, Kolatt, Primack, & Somerville 2001, ApJ, 550, 21

Dependence of Halo Concentration on Mass and Redshift

Profiles of dark haloes: evolution, scatter, and environment

J. S. Bullock[1,2], T. S. Kolatt[1,3], Y. Sigad[3], R.S. Somerville[3,4], A. V. Kravtsov[2,5★], A. A. Klypin[5], J. R. Primack[1], and A. Dekel[3] 2001 MNRAS 321, 559

ABSTRACT

We study dark-matter halo density profiles in a high-resolution N-body simulation of a ΛCDM cosmology. Our statistical sample contains ∼5000 haloes in the range $10^{11} - 10^{14} h^{-1} M_{\odot}$ and the resolution allows a study of subhaloes inside host haloes. The profiles are parameterized by an NFW form with two parameters, an inner radius r_s and a virial radius R_{vir}, and we define the halo concentration $c_{vir} \equiv R_{vir}/r_s$. We find that, for a given halo mass, the redshift dependence of the median concentration is $c_{vir} \propto (1+z)^{-1}$. This corresponds to $r_s(z) \sim$ constant, and is contrary to earlier suspicions that c_{vir} does not vary much with redshift. The implications are that high-redshift galaxies are predicted to be more extended and dimmer than expected before. Second, we find that the scatter in halo profiles is large, with a 1σ $\Delta(\log c_{vir}) = 0.18$ at a given mass, corresponding to a scatter in maximum rotation velocities of $\Delta V_{max}/V_{max} = 0.12$. We discuss implications for modelling the Tully-Fisher relation, which has a smaller reported intrinsic scatter. Third, subhaloes and haloes in dense environments tend to be more concentrated than isolated haloes, and show a larger scatter. These results suggest that c_{vir} is an essential parameter for the theory of galaxy modelling, and we briefly discuss implications for the universality of the Tully-Fisher relation, the formation of low surface brightness galaxies, and the origin of the Hubble sequence. We present an improved analytic treatment of halo formation that fits the measured relations between halo parameters and their redshift dependence, and can thus serve semi-analytic studies of galaxy formation.

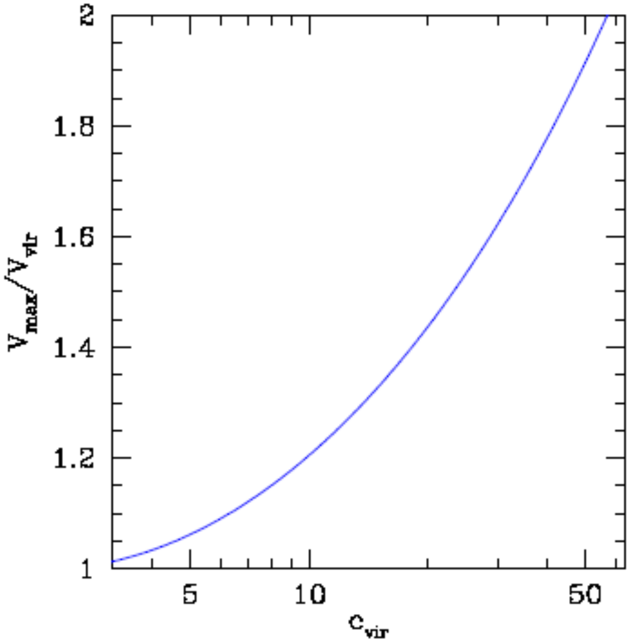

Figure 1. Maximum velocity versus concentration. The maximum rotation velocity for an NFW halo in units of the rotation velocity at its virial radius as a function of halo concentration.

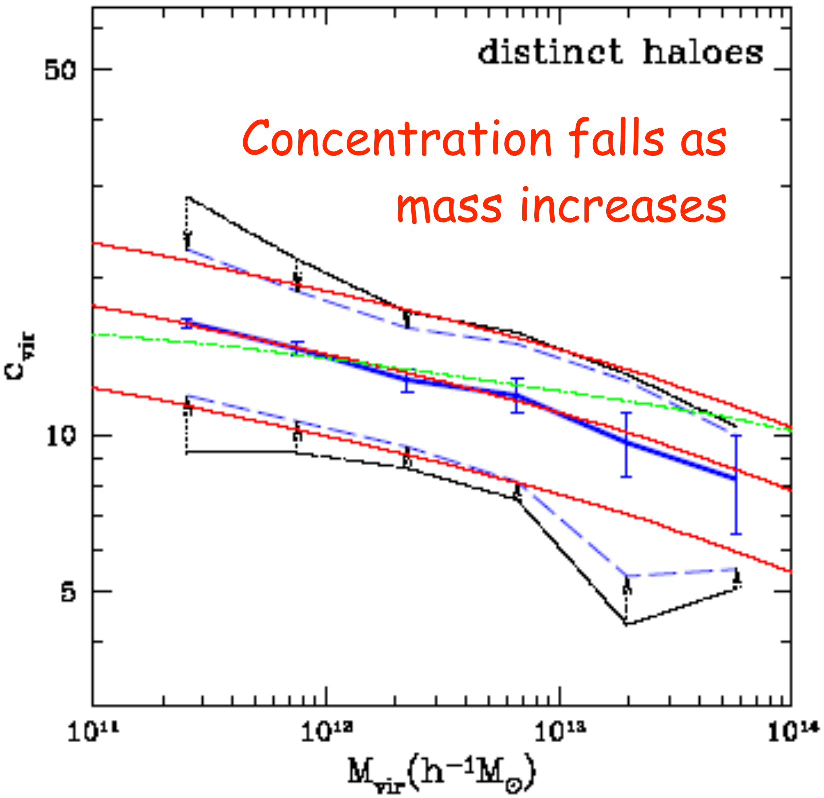

Figure 4. Concentration versus mass for distinct haloes at $z = 0$. The thick solid curve is the median at a given M_{vir}. The error bars represent Poisson errors of the mean due to the sampling of a finite number of haloes per mass bin. The outer dot-dashed curves encompass 68% of the c_{vir} values as measured in the simulations. The inner dashed curves represent only the true, intrinsic scatter in c_{vir}, after eliminating both the Poisson scatter and the scatter due to errors in the individual profile fits due, for example, to the finite number of particles per halo. The central and outer thin solid curves are the predictions for the median and 68% values by the toy model outlined in the text, for $F = 0.01$ and three different values of K. The thin dot-dashed line shows the prediction of the toy model of NFW97 for $f = 0.01$ and $k = 3.4 \times 10^3$.

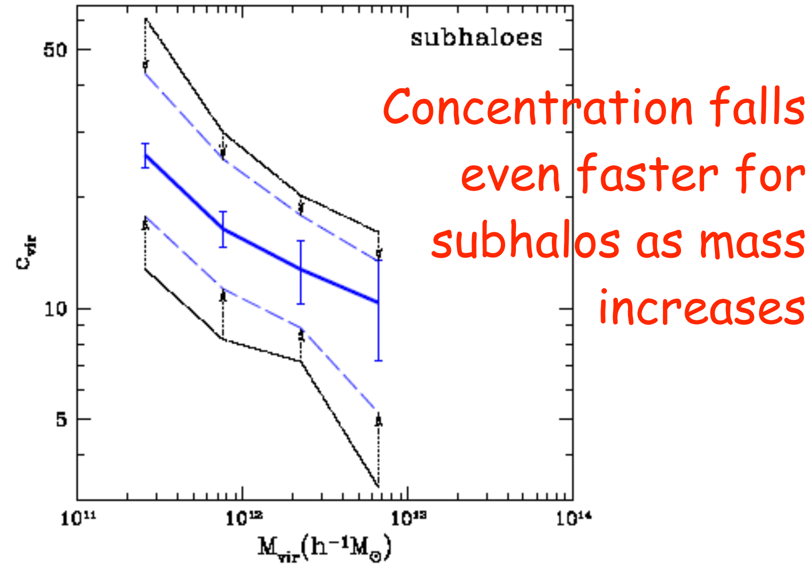

Figure 5. Concentration versus mass for subhaloes at $z = 0$. The curves and errors are the same as in Figure 4.

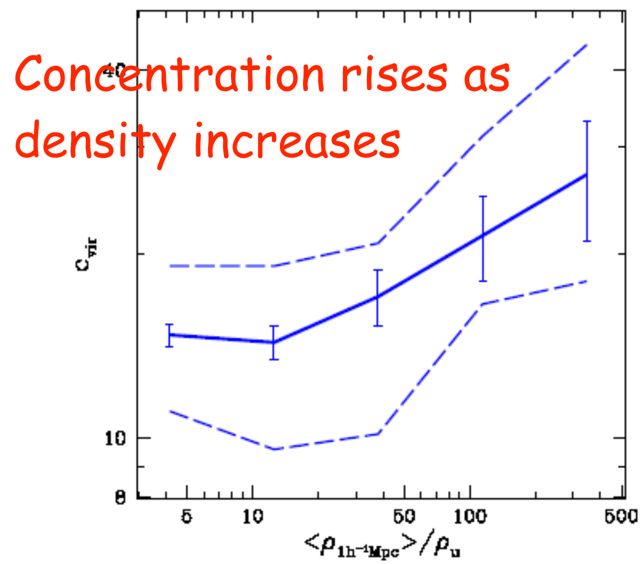

Figure 6. Concentrations versus environment. The concentration at $z = 0$ of all haloes in the mass range $0.5 - 1.0 \times 10^{12} h^{-1} M_{\odot}$ as a function of local density in units of the average density of the universe. The local density was determined within spheres of radius $1h^{-1}$Mpc. The solid line represents the median c_{vir} value, the error bars are Poisson based on the number of haloes, and the dashed line indicates our best estimate of the intrinsic scatter.

Spread of Halo Concentrations

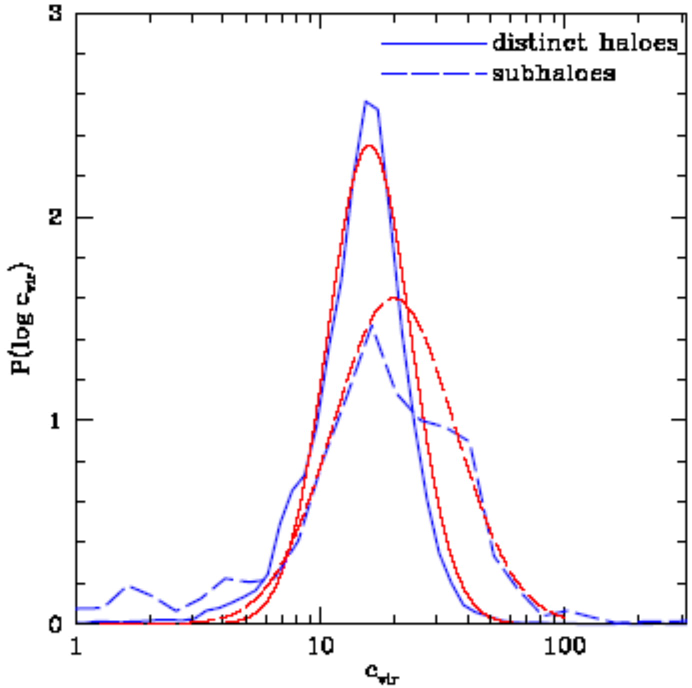

Figure 7. The probability distributions of distinct haloes (solid line) and subhaloes (dashed line) at $z = 0$ within the mass range $(0.5 - 1.0) \times 10^{12} h^{-1} M_{\odot}$. The simulated distributions (thick lines) include, the $\sim 2,000$ distinct haloes and ~ 200 subhaloes within this mass range. Log-normal distributions with the same median and standard deviation as the measured distributions are shown (thin lines). Subhaloes are, on average, more concentrated than distinct haloes and they show a larger spread.

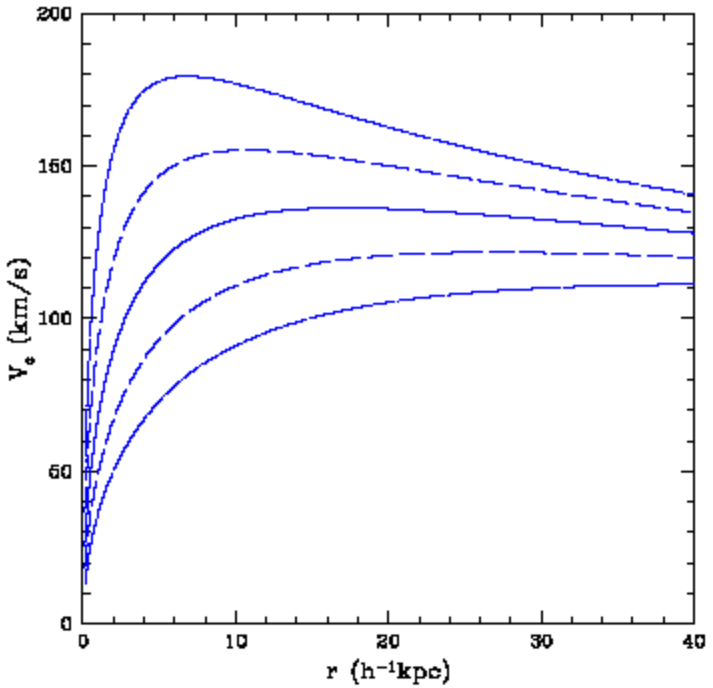

Figure 8. The spread in NFW rotation curves corresponding to the spread in concentration parameters for distinct haloes of $3 \times 10^{11} h^{-1} M_{\odot}$ at $z = 0$. Shown are the median (solid), $\pm 1\sigma$ (long dashed), and $\pm 2\sigma$ (dot-dashed) curves. The corresponding median rotation curve for subhaloes is comparable to the upper 1σ curve of distinct haloes.

Evolution of Halo Concentration with Redshift

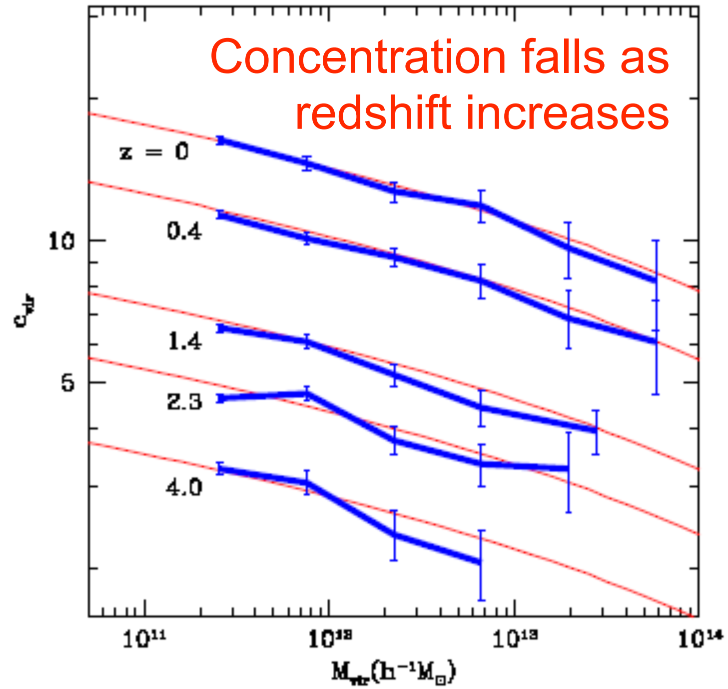

Figure 10. Median $c_{\rm vir}$ values as a function of $M_{\rm vir}$ for distinct haloes at various redshifts. The error bars are the Poisson errors due to the finite number of haloes in each mass bin. The thin solid lines show our toy model predictions.

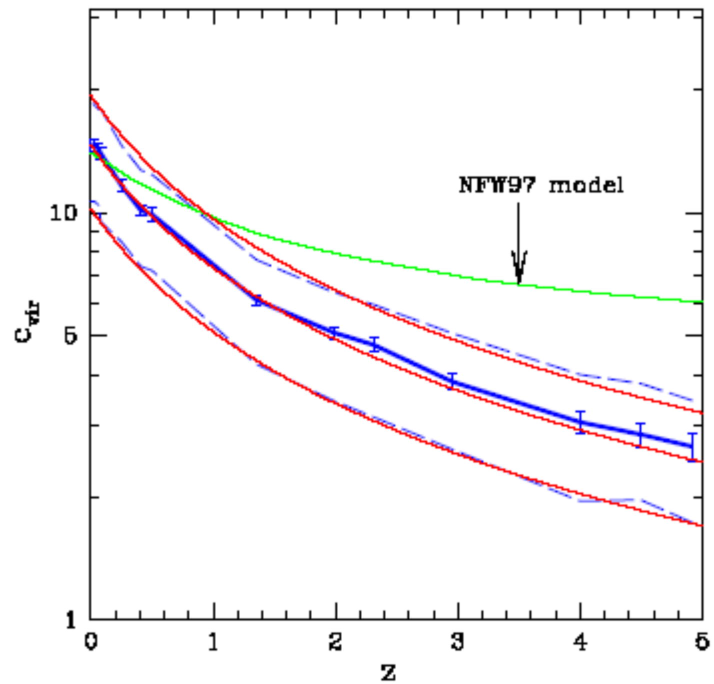

Figure 11. Concentration as a function of redshift for distinct haloes of a fixed mass, $M_{\rm vir} = 0.5 - 1.0 \times 10^{12} h^{-1} M_{\odot}$. The median (heavy solid line) and intrinsic 68% spread (dashed line) are shown. The behavior predicted by the NFW97 toy model is marked. Our revised toy model for the median and spread for $8 \times 10^{11} h^{-1} M_{\odot}$ haloes (thin solid lines) reproduces the observed behavior rather well.

$C_{vir} \propto 1/(1+z)$
at fixed mass

Merger Trees

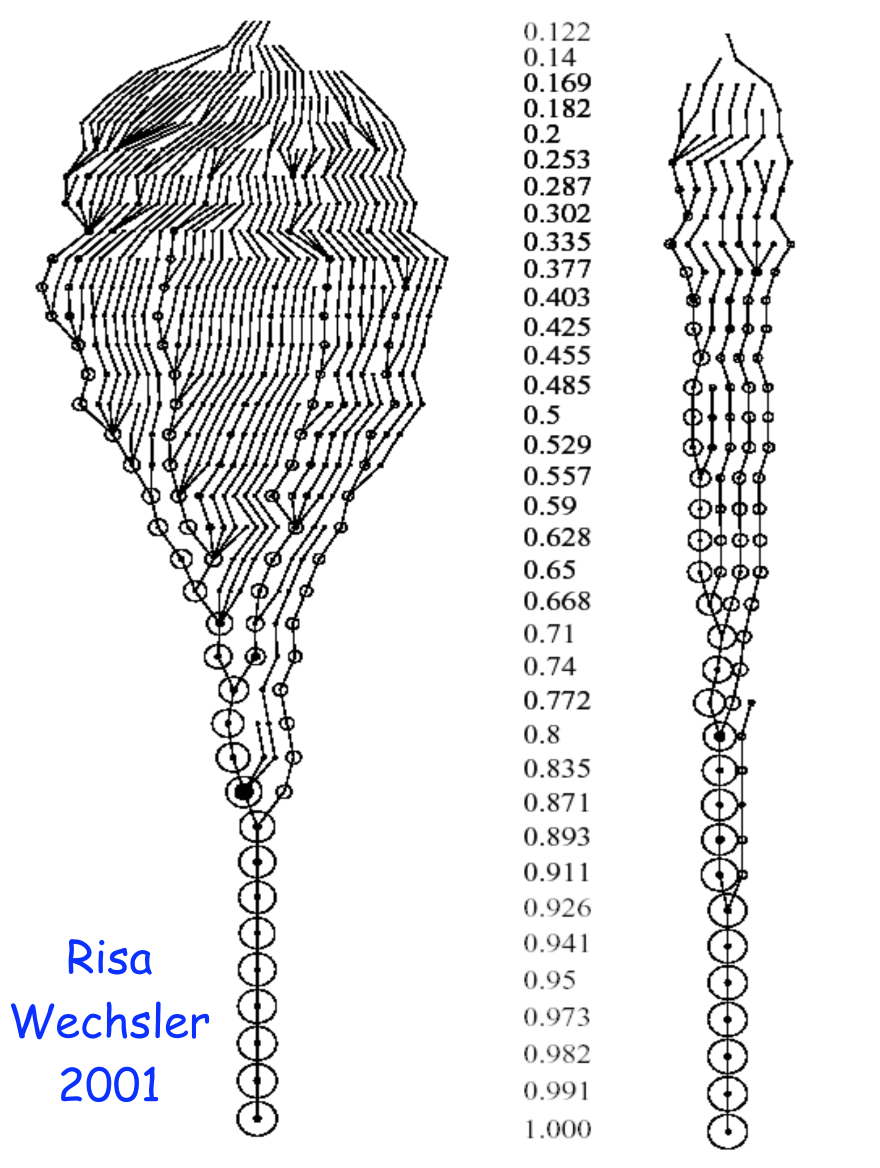

Risa Wechsler 2001

Based on our ART simulations, Wechsler created the first structural merger trees tracing the merging history of thousands of halos with structural information on their higher-redshift progenitors, including their radial profiles and spins. This led to the discovery that a halo's merging history can be characterized by a single parameter a_c which describes the scale factor at which the halo's mass accretion slows, and that this parameter correlates very well with the halo concentration, thus showing that the distribution of dark matter halo concentrations reflects mostly the distribution of their mass accretion rates. We found that the radius of the inner part of the halo, where the density profile is roughly 1/r, is established during the early, rapid-accretion phase of halo growth (a result subsequently confirmed and extended by other groups, e.g., Zhao et al. 2003, Reed et al. 2004).

CONCENTRATIONS OF DARK HALOS FROM THEIR ASSEMBLY HISTORIES

Risa H. Wechsler[1], James S. Bullock[2], Joel R. Primack[1], Andrey V. Kravtsov[2,3], Avishai Dekel[4], ApJ 568 (2002) 52-70

$$\rho_{\rm NFW}(r) = \frac{\rho_s}{(r/R_s)\,(1 + r/R_s)^2}, \qquad (1)$$

where R_s is a characteristic "inner" radius, and ρ_s a corresponding inner density. One of the inner parameters can be replaced by a "virial" parameter, either the virial radius ($R_{\rm vir}$), mass ($M_{\rm vir}$), or velocity ($V_{\rm vir}$), defined such that the mean density inside the virial radius is $\Delta_{\rm vir}$ times the mean universal density ρ_u at that redshift:

$$M_{\rm vir} \equiv \frac{4\pi}{3}\Delta_{\rm vir}\rho_u {R_{\rm vir}}^3. \qquad (2)$$

The critical overdensity at virialization, $\Delta_{\rm vir}$, is motivated by the spherical collapse model; it has a value $\simeq 180$ for the Einstein-deSitter cosmology, and $\simeq 340$ for the ΛCDM cosmology assumed here. A useful alternative parameter for describing the shape of the profile is the concentration parameter $c_{\rm vir}$, defined as $c_{\rm vir} \equiv R_{\rm vir}/R_s$.

(Bryan & Norman 1998) $\Delta_{\rm vir} \simeq (18\pi^2 + 82x - 39x^2)/\Omega(z)$
where $x \equiv \Omega(z) - 1$

By examining a range of full mass assembly histories for our sample of halos, we have found a useful parameterized form that captures many essential aspects of halo growth over time. Remarkably, we find that both average mass accretion histories and mass accretion histories for individual halos, as observed at $z = 0$, can be characterized by a simple function:

$$M(a) = M_o e^{-\alpha z}, \quad a = (1+z)^{-1}. \qquad (3)$$

The single free parameter in the model, α, can be related to a characteristic epoch for formation, a_c, defined as the expansion scale factor a when the logarithmic slope of the accretion rate, $d\log M/d\log a$, falls below some specified value, S. The functional form defined in Eq. 3 implies $a_c = \alpha/S$. In what follows we have chosen $S = 2$.

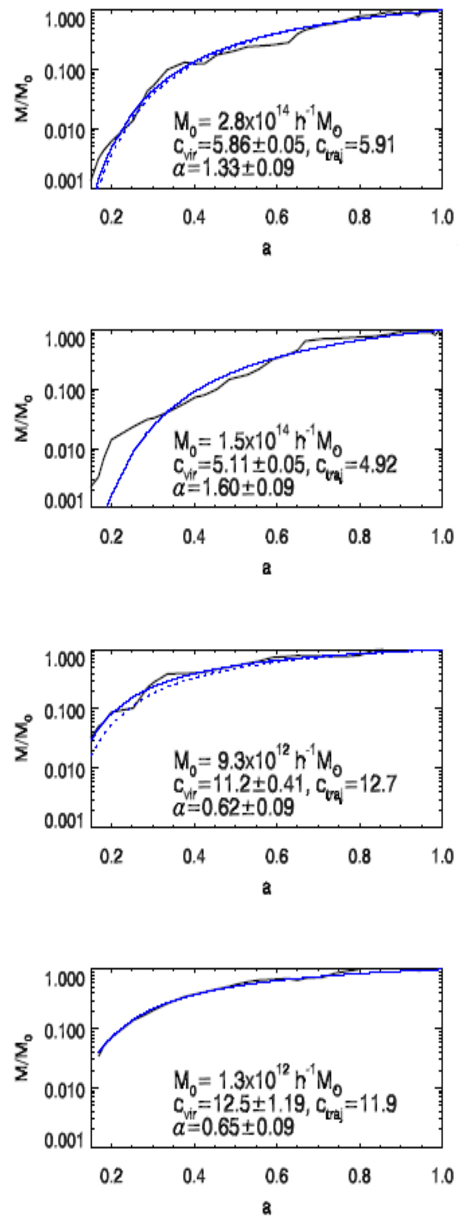

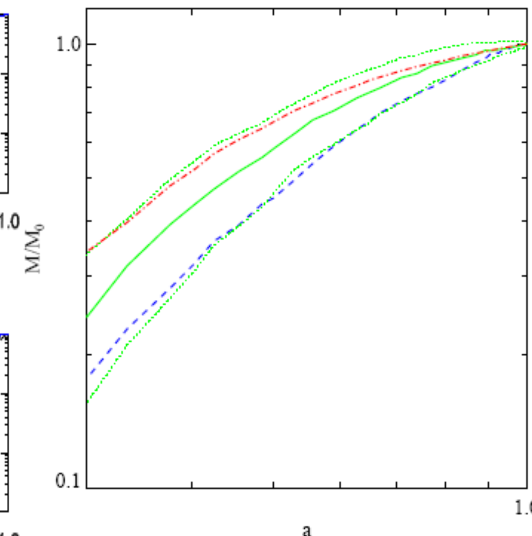

Average mass accretion histories, normalized at a = 1. The three green curves connect the averages of M(a)/M0 at each output time. The pair of dotted lines shows the 68% spread about the middle case. Red dot-dashed lines correspond to early formers (typically low mass halos), blue dashed lines to late formers (typically higher mass halos). We see that massive halos tend to form later than lower mass halos, whose mass accretion rate peaks at an earlier time.

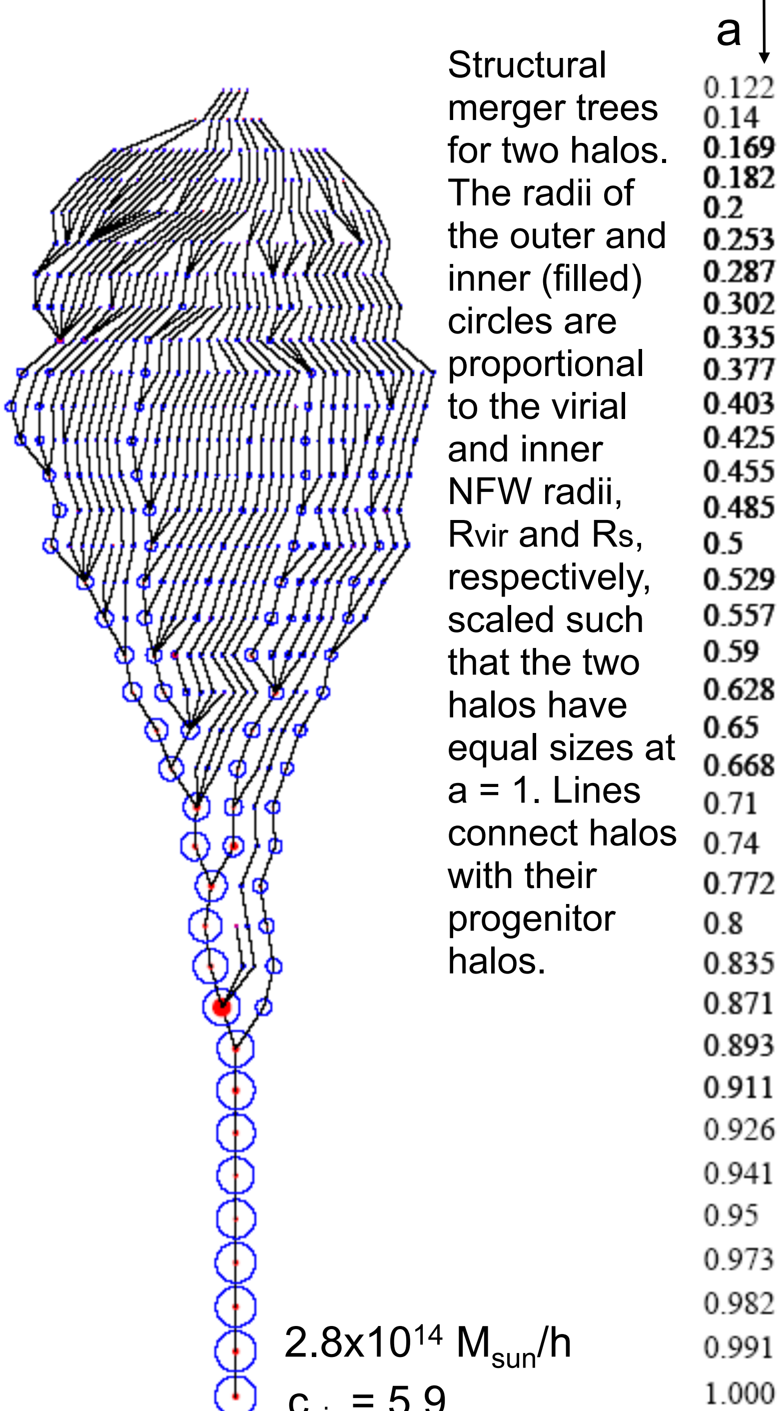

Structural merger trees for two halos. The radii of the outer and inner (filled) circles are proportional to the virial and inner NFW radii, Rvir and Rs, respectively, scaled such that the two halos have equal sizes at a = 1. Lines connect halos with their progenitor halos.

2.8×10^{14} M_{sun}/h
$c_{vir} = 5.9$

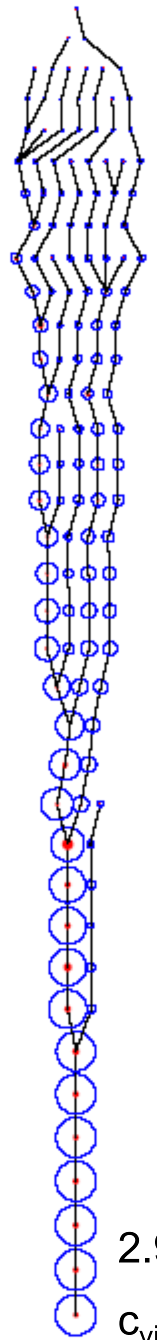

2.9×10^{12} M_{sun}/h
$c_{vir} = 12.5$

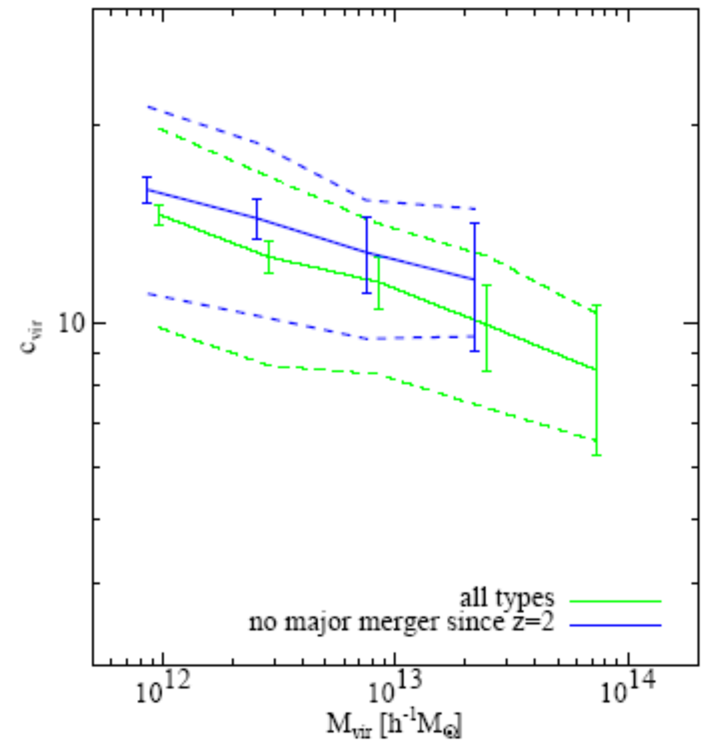

For halos without recent mergers, c_{vir} is higher and the scatter is reduced to $\log c_{vir} \approx 0.10$.

Wechsler et al. 2002

Halo Shapes

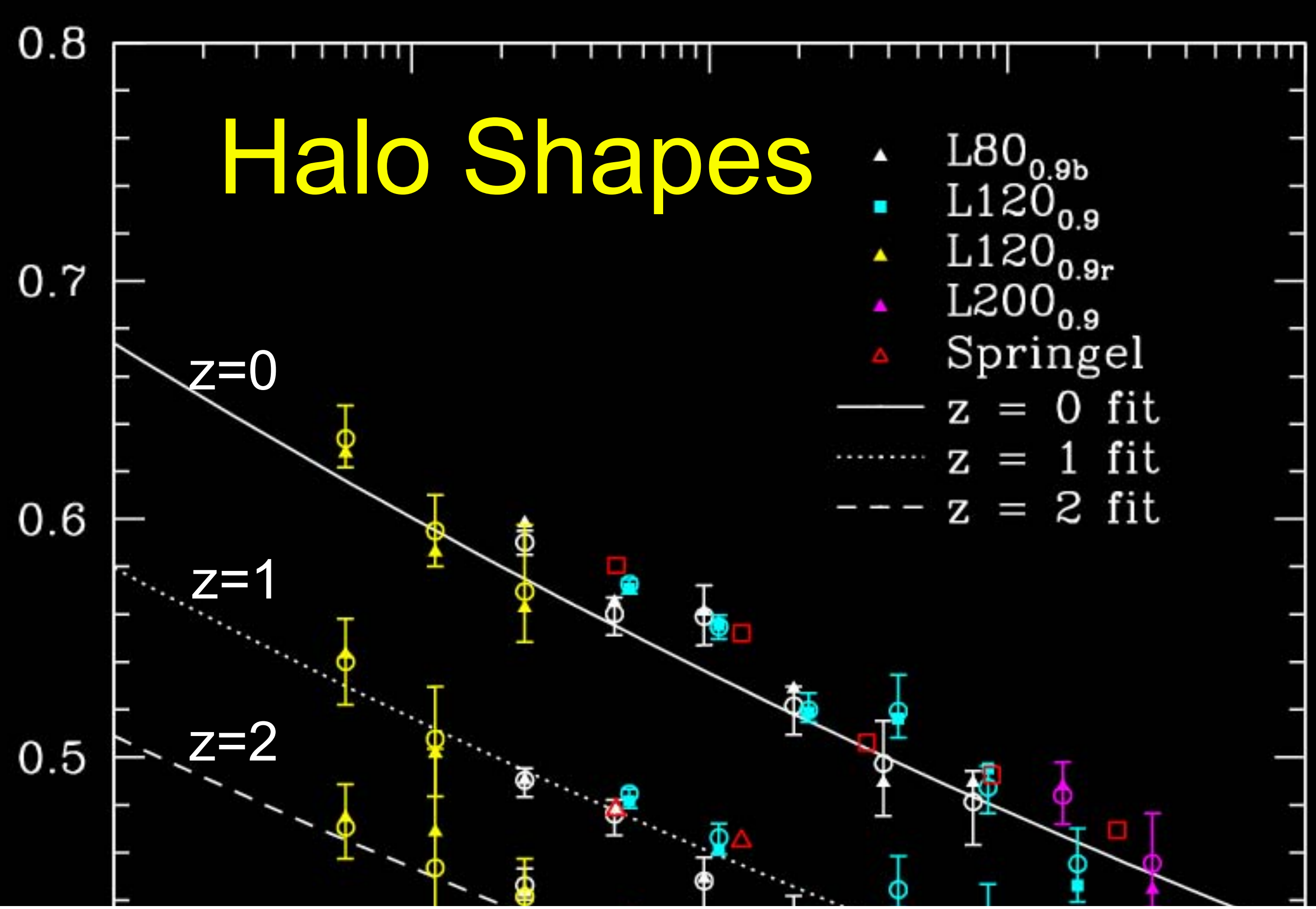

A simple formula describes these results, as well dependence on epoch and cosmological parameter σ_8 :

$$\langle s \rangle (M_{\rm vir}, z=0) = \alpha \left(\frac{M_{\rm vir}}{M_*} \right)^{\beta}$$

with best fit values

$$\alpha = 0.54 \pm 0.03, \ \beta = -0.050 \pm 0.003.$$

<s> = short / long axis of dark halos vs. mass and redshift. Dark halos are more elongated the more massive they are and the earlier they form. We found that the halo <s> scales as a power-law in Mhalo/M*. Halo shape is also related to the Wechsler halo formation scale factor ac.

Allgood et al. 2006

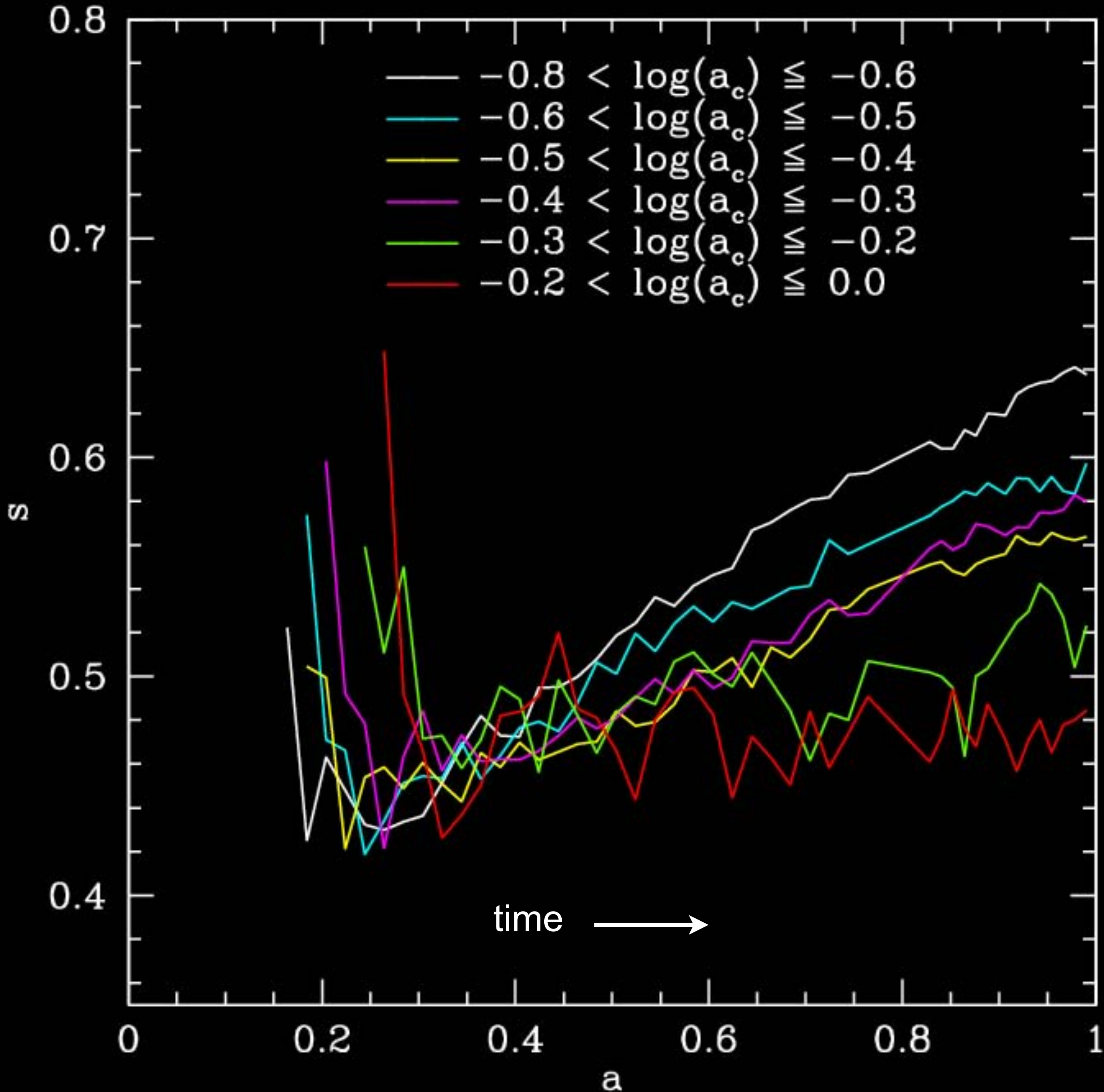

Halo shape $s = c / a$ vs. scale factor $a=1/(1+\text{redshift})$ for halos of mass between 3.2 and 6.4 x 10^{12} M_{sun} that form at different scale factors a_c. Halos become more spherical after they form, and those that form earlier (at lower a_c) become more spherical faster.

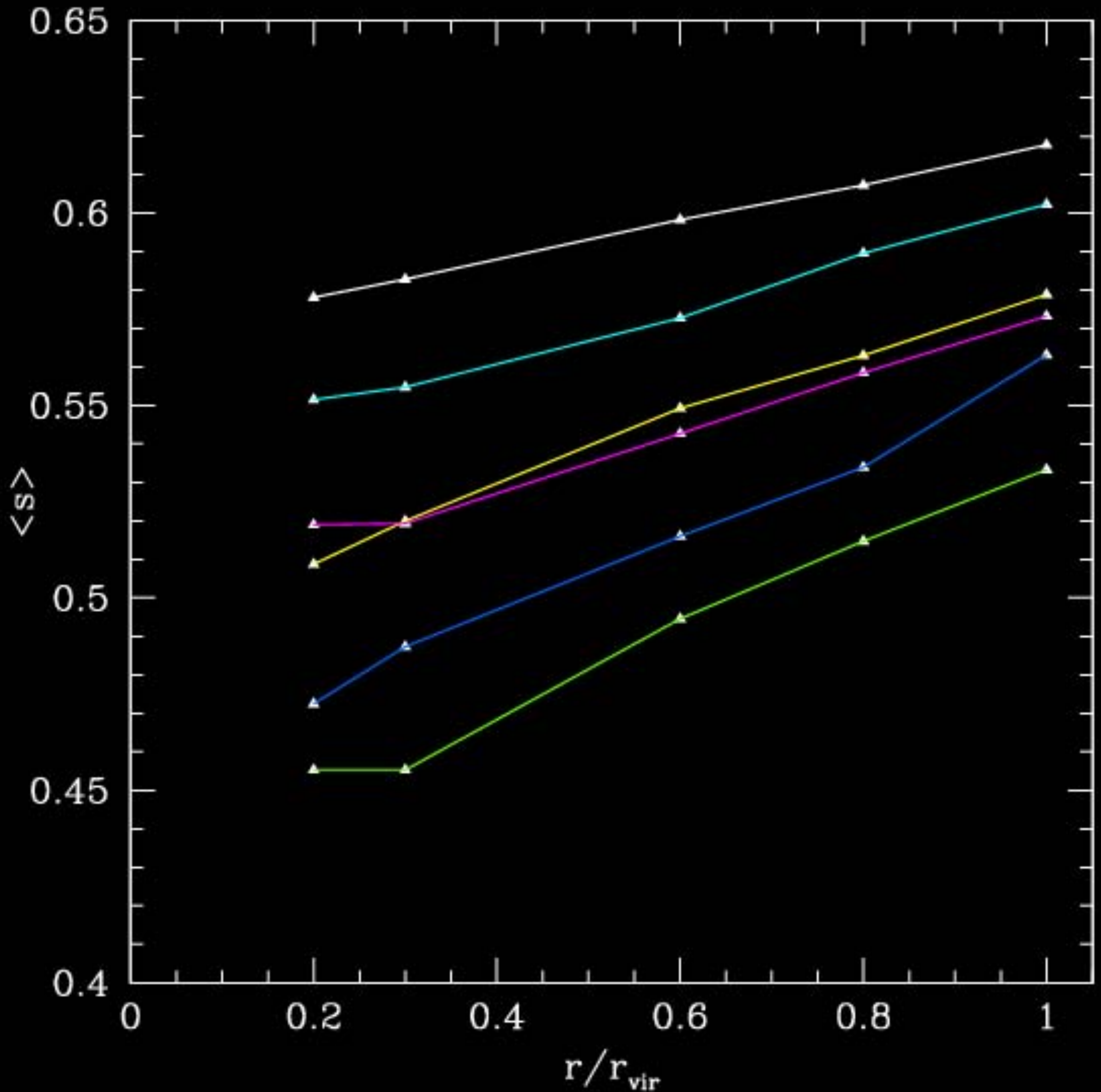

FIG. 7.— $\langle s \rangle$ with radius at $z = 0$. black: $1.6 \times 10^{12} < M < 3.2 \times 10^{12}$, red: $3.2 \times 10^{12} < M < 6.4 \times 10^{12}$, blue: $6.4 \times 10^{12} < M < 1.28 \times 10^{13}$, green: $1.28 \times 10^{13} < M < 2.56 \times 10^{13}$, orange: $2.56 \times 10^{13} < M < 5.12 \times 10^{13}$, violet: $5.12 \times 10^{13} < M$. These are the same mass bins as in Figure 3.

Halos become more spherical at larger radius and smaller mass. As before, s = short / long axis. These predictions can be tested against cluster X-ray data and galaxy weak lensing data.

[These figures are from Brandon Allgood's PhD dissertation.]

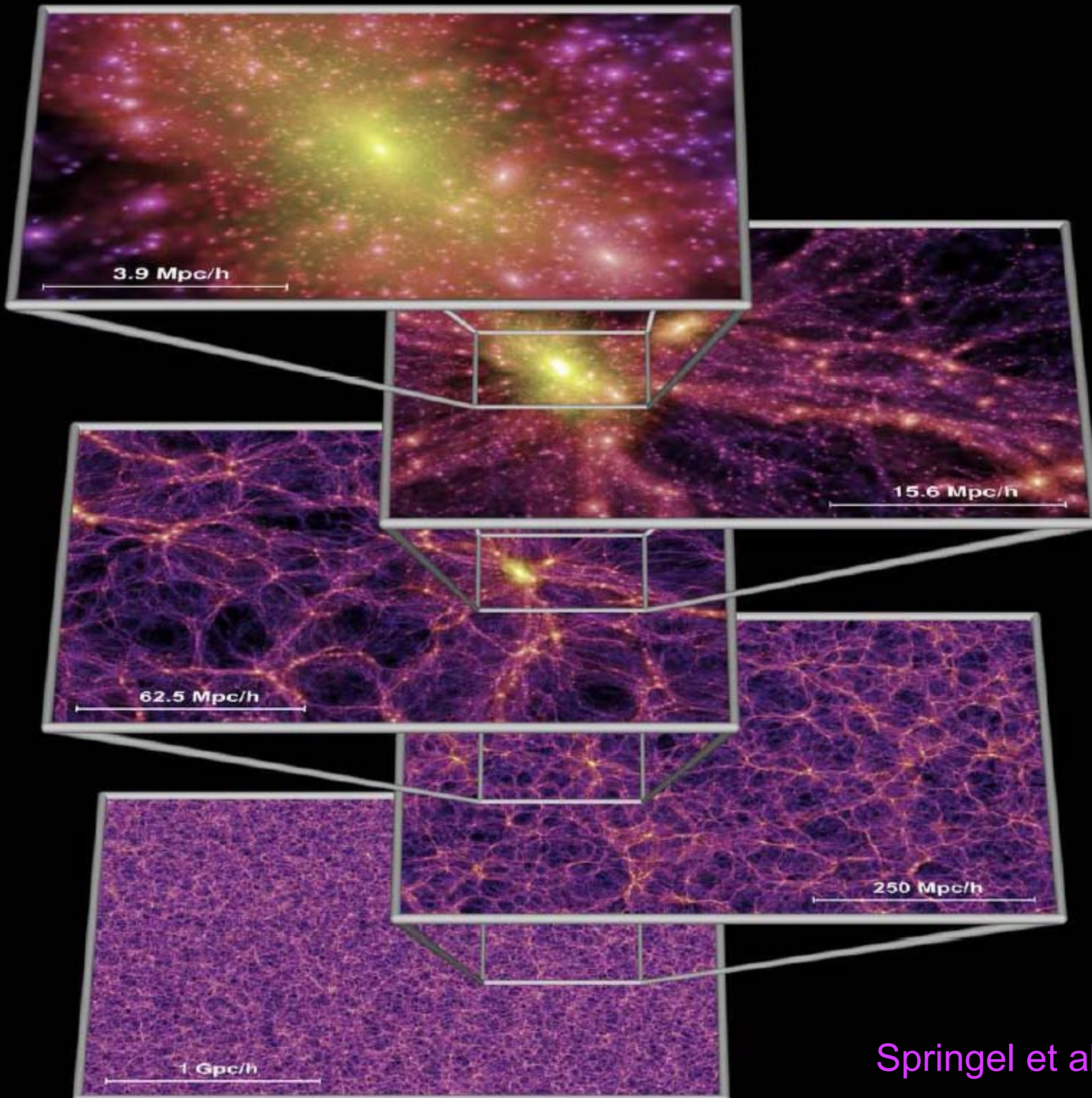

Springel et al. 2005

Particle number in cosmological N-body simulations vs. pub date

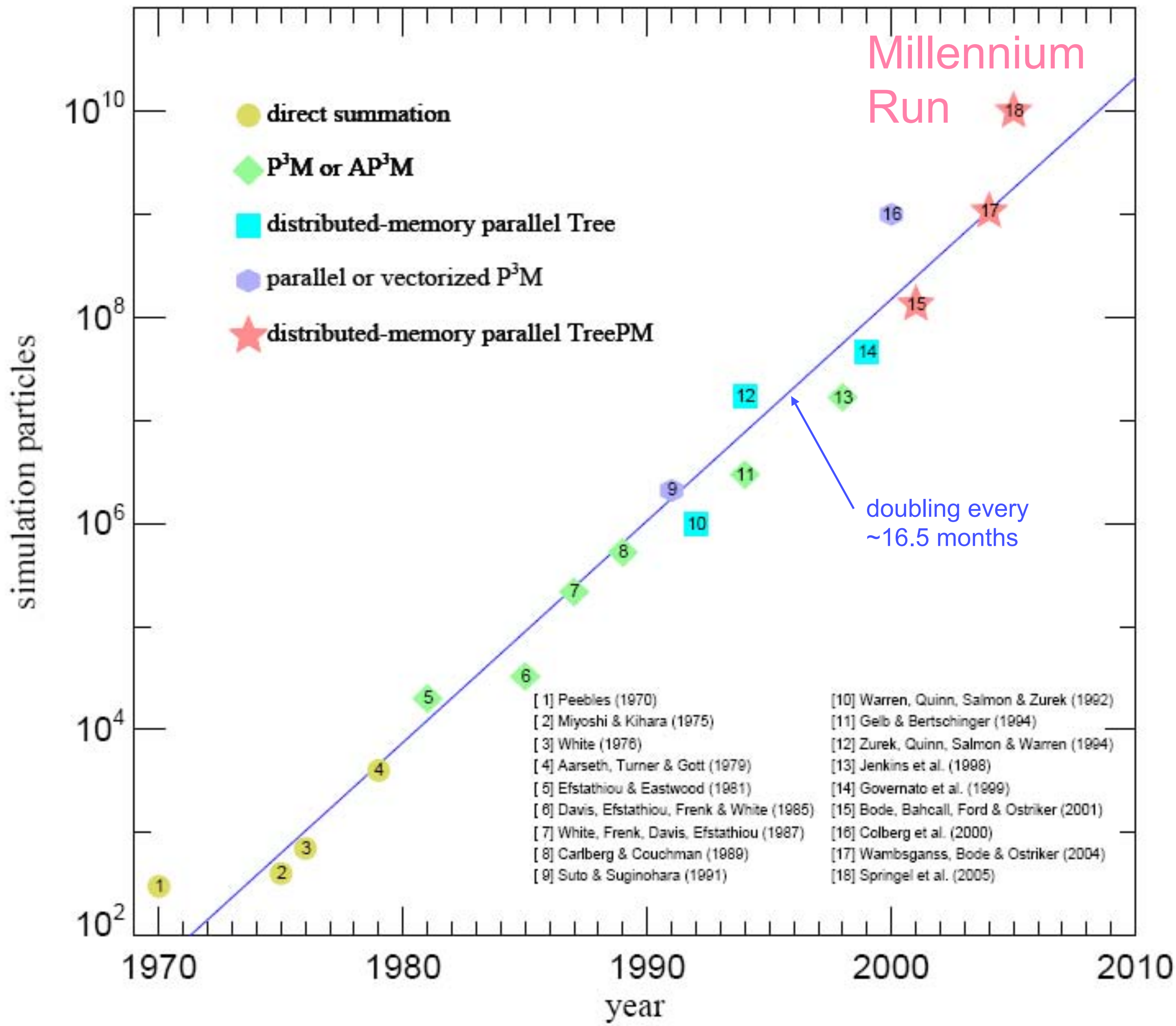

UNDERSTANDING GALAXY CORRELATIONS

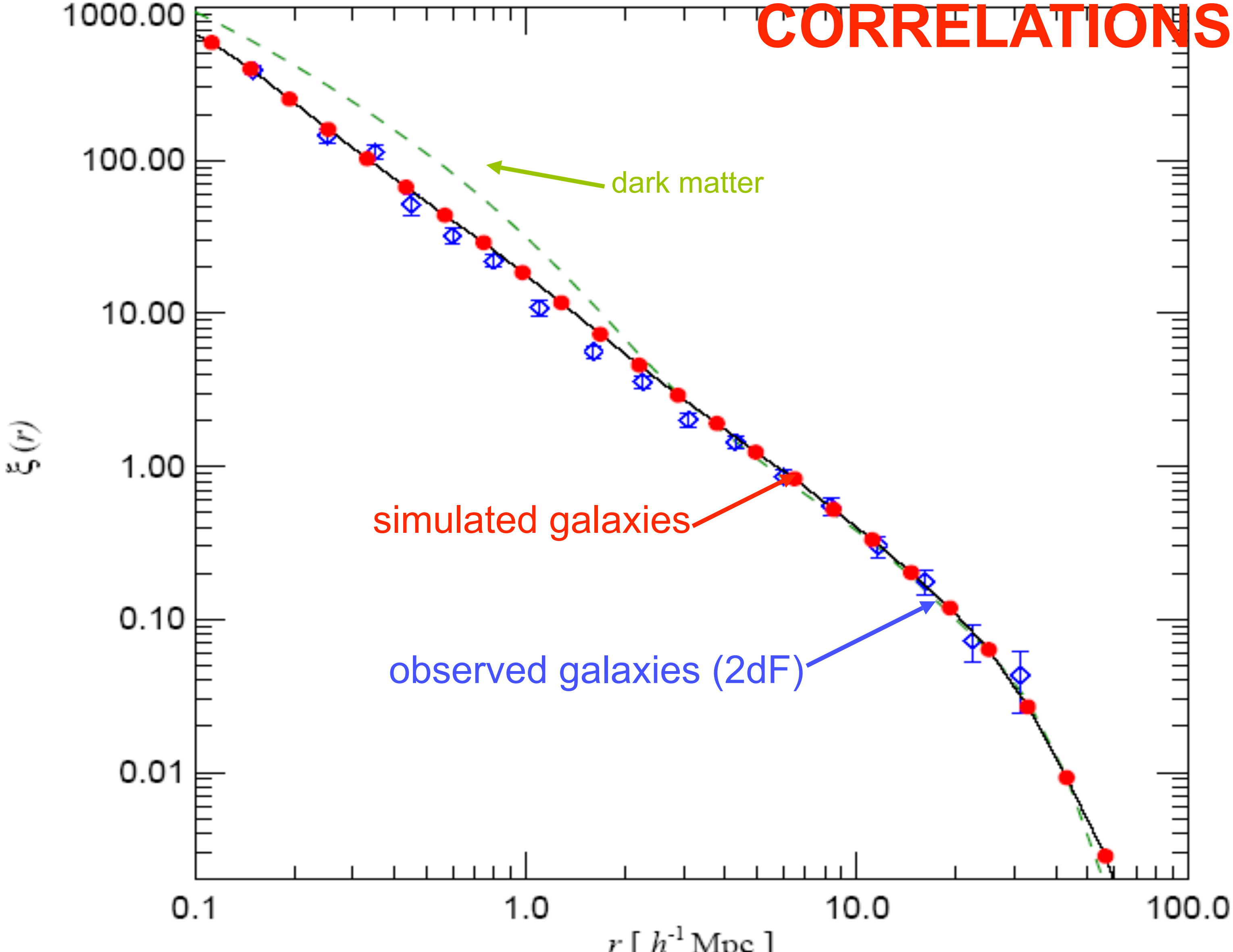

Galaxy 2-point correlation function at the present epoch.

Springel et al. 2005

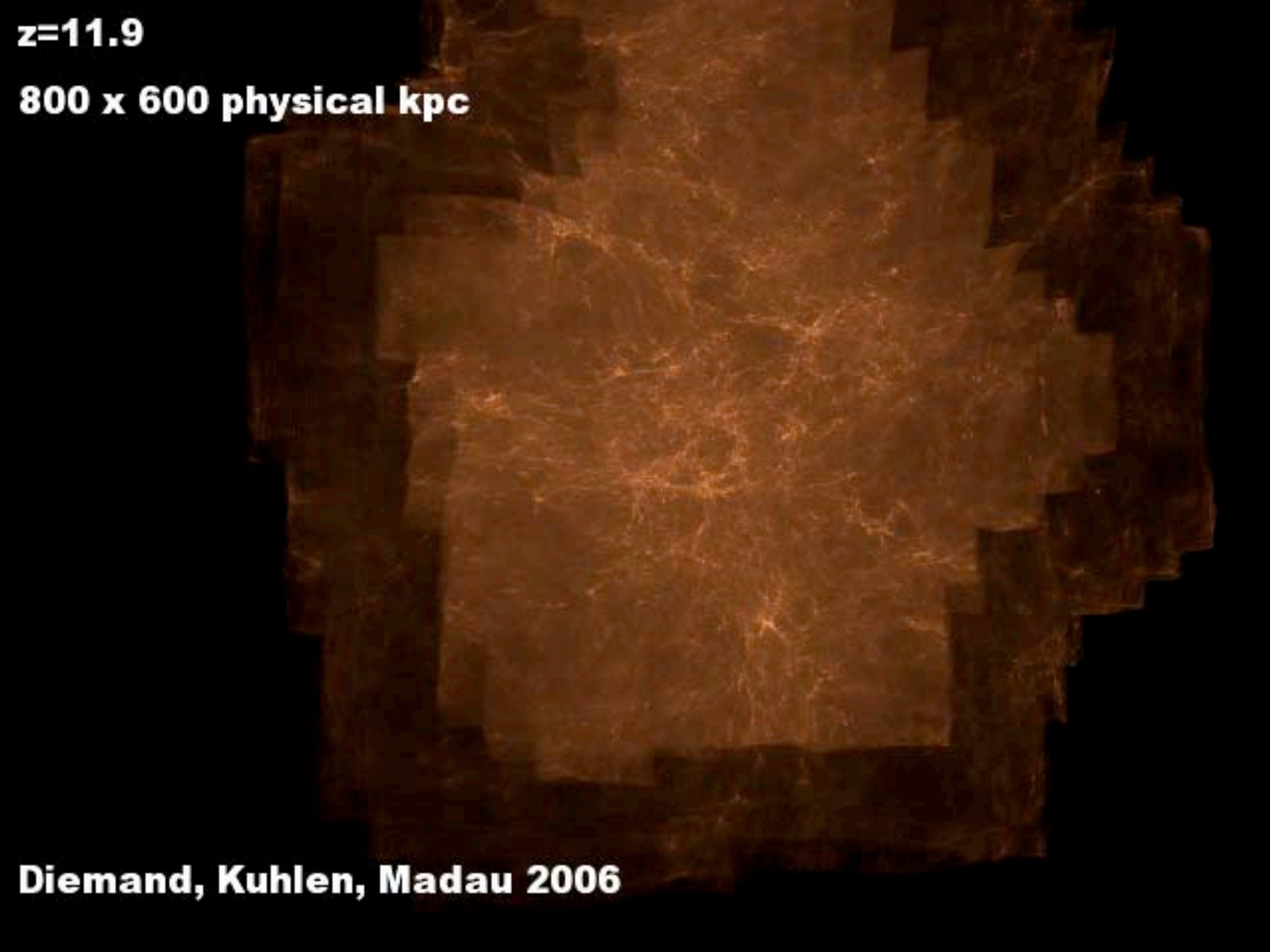
z=11.9
800 x 600 physical kpc
Diemand, Kuhlen, Madau 2006

Whatever Happened to Hot Dark Matter?

In ~1980, when purely baryonic adiabatic fluctuations were ruled out by the improving upper limits on CMB anisotropies, theorists led by Zel'dovich turned to what we now call the HDM scenario, with light neutrinos making up most of the dark matter. However, in this scheme the fluctuations on small scales are damped by relativistic motion ("free streaming" of the neutrinos until T becomes less than m_ν, which occurs when the mass entering the horizon is about 10^{15} solar masses, the supercluster mass scale. Thus superclusters would form first, and galaxies later by fragmentation. This predicted a galaxy distribution much more inhomogeneous than observed.

Since 1984, the most successful structure formation scenarios have been those in which most of the matter is CDM. With the COBE CMB data in 1992, two CDM variants appeared to be viable: ΛCDM with $\Omega_m \approx 0.3$, and $\Omega_m = 1$Cold+Hot DM with $\Omega_\nu \approx 0.2$. A potential problem with ΛCDM was that the correlation function of the dark matter was higher around 1 Mpc than the power-law $\xi_{gg}(r) = (r/r_0)^{-1.8}$ observed for galaxies, so "scale-dependent anti-biasing" was required (Klypin, Primack, & Holtzman 1996, Jenkins et al. 1998). A potential problem with CHDM was that, like all $\Omega_m = 1$ theories, it predicted rather late structure formation.

By 1998, the evidence of early galaxy and cluster formation and the increasing evidence that $\Omega_m \approx 0.3$ had doomed CHDM. But now we also know from neutrino oscillations that neutrinos have mass. The upper limit is $\Omega_\nu h^2 < 0.0076$ (95% CL), corresponding to $\Sigma\, m_\nu < 0.7$ eV (Spergel et al. 2003), with the slightly stronger constraint $\Sigma\, m_\nu < 0.4$ eV including Lyα forest data (Seljak et al. 2005).

ΛCDM Scale-Dependent Anti-Biasing

The dark matter correlation function ξ_{mm} for ΛCDM is $3\times\xi_{gg}$ at 1 Mpc. This disagreement was pointed out by Klypin, Primack, & Holtzman 1996. When simulations could resolve galaxy halos, it turned out that the needed anti-biasing arises naturally. This occurs because of destruction of halos in dense regions because of merging and tidal disruption.

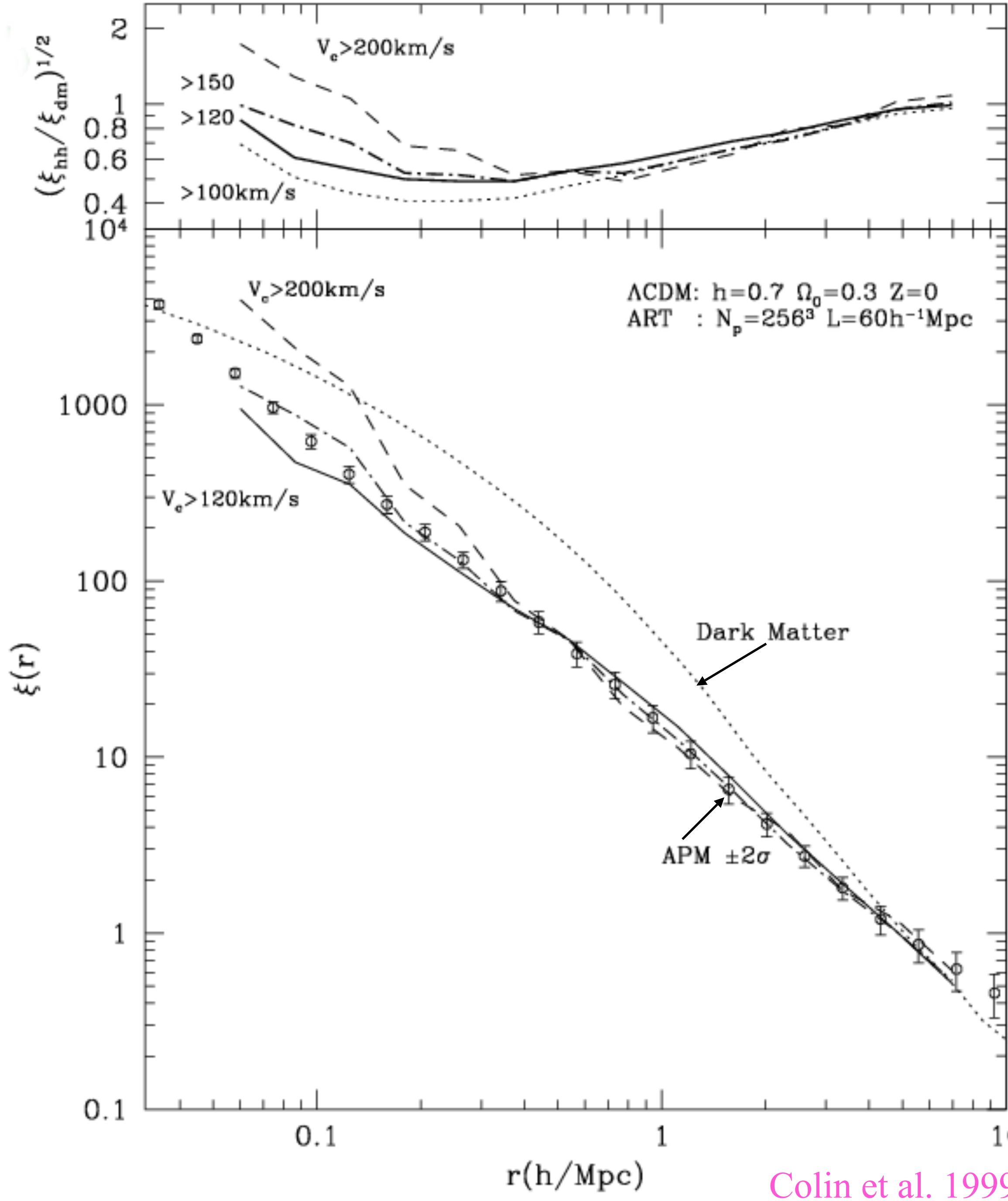

Colin et al. 1999